Copper exchanged FAU nanozeolite as non-toxic nitric oxide and carbon dioxide gas carrier

Kamila Goldyn, Clément Anfray, Sarah Komatya, Valerie Ruaux, Charly Hélaine, Richard Retoux, Samuel Valable, Valentin Valtchev, Svetlana Mintova

Copper exchanged FAU nanozeolite as non-toxic nitric oxide and carbon dioxide gas carrier

Kamila Goldyn [a‡], Clément Anfray [b‡], Sarah Komaty [a], Valerie Ruaux [a], Charly Hélaine [b], Richard Retoux [c], Samuel Valable [b], Valentin Valtchev [a] and Svetlana Mintova [a*]

[a.] Normandie Univ, ENSICAEN, CNRS, Laboratoire Catalyse et Spectrochimie, 14000 Caen, France

[b.] Normandie Univ, CEA, CNRS, GIP CYCERON, ISTCT/CERVOxy group, 14000 Caen, France

[c.] Normandie Univ, ENSICAEN, CNRS, CRISMAT, 14000 Caen, France

Abstract

A growing interest is currently directed to find an efficient NO and CO_2 gas carriers for biomedical applications. The gas adsorption properties of sodium- (Na-X) and copper- (Cu-X) containing FAU nanozeolite towards nitric oxide and carbon dioxide were studied. The materials were fully characterised by XRD, TEM, ICP, DLS and *in-situ* FTIR. The as-prepared Na-X showed higher gas adsorption ability towards carbon dioxide, whereas the ion-exchanged Cu-X was more efficient adsorbent with regards to nitric oxide. In addition, the cytotoxicity tests disclosed that both nanozeolites have no toxicity making them suitable for further tests in biomedical field as gas transporters.

Keywords: Metal-exchanged nanozeolites, gas adsorption, non-toxic, gas carrier, biomedical applications

Introduction

The well-established activity of copper containing zeolites with nitric oxide (NO) and carbon dioxide (CO_2) have proved their functionality mainly as a de-NOx catalyst, where the zeolites are used to perform selective catalytic reduction of nitric oxide (NO) [1–3], as well as CO_2 adsorbent for gas separation in industrial and environmental processes [4,5]. Based on this background we develop new application where zeolites are employed to act as NO and CO_2 gas carriers for potential biomedical applications.

NO is an antibacterial, principal signalling molecule (generated within the body), that is involved in many biological processes, namely regulation of the blood flow, neurotransmission and immune response [6–8]. CO_2, also generated within the body as a result of aerobic respiration, is an essential moderator in human physiology, controlling blood circulation and pH. The extrinsic delivery of such biologically active molecules is an interesting and challenging way of therapy that could potentially be an effective remedy for major illnesses. As an example, when CO_2 is inhaled in the form of carbogen (mixture of O_2 95% and 5 % CO_2), it increases tissue perfusion and oxygenation, which is an important stage in improving tumour treatment efficacy [9,10]. However, the broad range of effects generated in the body by these two gases raised an issue about its specificity and targeted delivery, which complicated the progress for their applications in biomedicine. Therefore, to overcome those uncertainties, the development of selective and most importantly non-toxic materials that can carry and release therapeutic gases is required.

Nowadays, there is a growing interest in finding suitable NO carriers to prevent perilous life conditions such as thrombosis (blood clot formation), at the surface of artificial blood vessels and medical devices. Currently, anticoagulants such as heparin

are employed to overcome thrombosis, however, the use of latter can cause unexpected bleeding in other parts of the body, leading to loss of platelets and thus thrombocytopenia [11]. In the case of carbogen administration, the inhalation via nasal cannula or facemask showed insufficiency on tissue reoxygenation regarding progressive response to radio therapy [12]. As a result, a vast number of NO- and CO_2-carrying materials have been proposed, which are mainly based on synthetic polymers (PVC, PDMS) and fumed silica particles. For NO delivery purposes those materials have been functionalised with various amines, and upon reaction with NO, they form diazeniumdiolate ions. The latter, can hydrolyse in aqueous solution with suitable pH to release nitric oxide and thus act as a gas donor [13–17]. Over the years, it was demonstrated, namely by the group of Morris *et al.* that metal exchanged, highly crystalline porous materials, such as zeolites and metal organic framework (MOFs) type materials have the ability to adsorb and release nitric oxide [18–21]. The adsorption of CO_2 in zeolites was also studied widely and demonstrated they can be used for an efficient gas storage and delivery for both environmental and biomedical applications [18,22–24]. The characteristics of zeolites namely, well-defined porous structures, high specific surface area, and chemical/thermal stability render them as appropriate materials for selective gas adsorption purposes [25,26]. Additionally, the chemical properties of zeolites, enable to control the gas adsorption capacity, which can be accomplished by tuning the zeolite composition, in terms of the type of metal ion present in the structure. The introduction of various cations (Fe^{3+}, Ce^{3+} Cu^{2+}, Gd^{3+}) in the zeolite is usually achieved via post-synthetic ion-exchange, to further functionalise the material for targeted application [27,28]. Other aspects influencing the gas sorption

affinity are the zeolite physical features, such as size and framework type (more than 239), providing a great array of structures to choose from depending on desired use.

The low toxicity of zeolite plays a major role when it comes to biomedical applications. The modifications of zeolite crystal size, from micron to nanoscale, as well as the development of template-free synthesis, yielding biocompatible nanozeolites becomes of important research field. The cytotoxicity of nanozeolites does not just depend on crystal size but also on particle agglomeration and stability in colloidal suspension [29]. As a result of their low toxicity towards sensitive cells (such as cells from the central nervous system), nanocrystals have drawn particular attention of researches working in the field of biomedical science, especially for contrast agents, controlled drug release [30–32], and gas delivery purposes [28,33,34]. Moreover, it has recently been reported that the copper containing FAU nanozeolite (in form of stable suspension), can be used for direct sanitisation of medical surfaces against ESKAPE bacteria and thus act as antimicrobial agent to prevent life-threatening infections.[35]

Here, we report the preparation of sodium and copper containing FAU-type nanozeolite (zeolite X) with high sorption capacity towards NO and CO_2, which can be used as alternative way of gas delivery for biomedical applications. The sorption affinity of as prepared Na- containing FAU (Na-X) and Cu ion-exchanged zeolite (Cu-X) to NO and CO_2 was studied by *in-situ* IR spectroscopy. Moreover, the cytotoxicity tests using a selection of cells, including, human tumour, kidney and most sensitive primary culture of astrocytes to assess the biocompatibility of prepared nanozeolites were performed. We also demonstrated that the cation types in zeolites highly affect the gas adsorption properties, i.e., the Cu-X has greater adsorption capacity towards NO, whereas the as prepared Na-X has higher CO_2 sorption affinity. The high sorption

capacity of non-toxic Cu-X, combined with antimicrobial properties, provide a platform for alternative therapies in the biomedical field.

2 Experimental

2.1. Preparation of Cu-FAU nanozeolite

The template-free, nanosized Na-X zeolite with FAU framework topology was synthesised following a previously reported procedure [36]. The aluminate solution consisted of 2.5 g of sodium hydroxide (NaOH, 97 %, Sima-Aldrich) which was dissolved in 3.0 g double distilled water (dd H_2O), followed by slow addition of 0.297 g aluminum powder (325 mesh, 99.5 %, Alfa Aesar). The mixture was stirred until a clear solution was obtained. The silicate solution was prepared by dissolving 1.1 g of NaOH in 1.0 g of dd H_2O, followed by the addition of 10 g colloidal silica (Ludox-HS 30, 30 wt % SiO_2, Aldrich). The acquired white, turbid suspension was placed in the oven at 100 °C for 5 min to obtain a clear suspension. The aluminate solution was then added dropwise to the latter placed in an ice-bath under vigorous stirring. As a result, a clear suspension with the starting molar composition 9 Na_2O: 1.1 Al_2O_3: 10 SiO_2: 122 H_2O was produced, then aged at room temperature for 24 h, followed by dehydration (to adjust the H_2O content to 45) and hydrothermal treatment at 50 °C for 26 h. The crystalline product were recovered by centrifugation (20000 rpm, 25 min) and purified by washing with dd H_2O until reaching the pH= 7.

The Cu-X was prepared by ion-exchange of 2.4 wt % Na-X suspension with 0.004 M of copper nitrate (Cu $(NO_3)_2.9H_2O$) at room temperature for 1 h (zeolite to copper

suspension ratio 1:5). The sample was washed three times by centrifugation (20000 rpm, 25 min) and redispersed in dd H_2O. The final pH of the Cu-X suspension was 7.

2.2. Characterisation

The stability and particle size distribution of Na-X and Cu-X zeolite suspensions (pH= 7) was determined by zeta potential and dynamic light scattering (DLS) respectively, using a Malvern Zetasizer Nano instrument. The crystal structure of the parent Na-X and the ion-exchanged zeolite Cu-X was determined by X-ray diffraction. The analyses were performed with a PANalytical X'Pert PRO-MPD diffractometer with Cu Kα radiation (λ = 1.5418 Å). The samples were scanned in the 2θ range of 4-50° with a step size of 0.016°. The size and morphology of zeolites were studied by scanning electron microscope (SEM, MIRA-LMH TESCAN) supplied with a field emission gun and a transmission electron microscopy (TEM, 200 kV JEOL 2010 FEG). The elemental composition was determined by inductively coupled plasma-atomic emission spectroscopy (ICP-AES) using an OPTIMA 4300 DV (PerkinElmer) instrument.

The adsorption capacities of self-supported zeolites wafers (2 cm^2 area, 20 mg) towards NO and CO_2 were determined using Nicolet Magna 550-FTIR spectrometer (4 cm^{-1} optical resolution and 128 scans) equipped with MCT detector. Prior to the adsorption measurements, each sample was activated at 120 °C under oxygen for 4 hours, followed by evacuation at the same temperature. The sample was further heated for 4h at 300 °C under vacuum (10^{-6} Torr). The NO and CO_2 were adsorbed at room temperature using various amounts introduced in small volumes; 1-100 Torr for NO and 10-180 Torr for CO_2. All spectra were normalised to the sample weight.

2.3. Cytotoxicity tests: materials and methods

Cell lines: Human embryonic kidney (HEK 293) and human glioblastoma cells (U87-MG), were cultured in DMEM (Sigma-Aldrich, France) prior the toxicity tests. The cell lines listed above were purchased from ATCC (Manassas, VA, USA) and maintained in culture at 37°C with 5% CO_2 and 95% humidity.

DMEM was supplemented with 10% foetal bovine serum (Eurobio, France), 2 mM glutamine (Sigma-Aldrich, France) and 100 U/ml penicillin/streptomycin (Sigma-Aldrich, France).

Primary culture of astrocytes: Cerebral cortices (isolated from neonatal 1-3 days old mice, Swiss, CURB, France) were carefully stripped of the meninges and dissociated to generate a single-cell suspension. The cultures were left to grow in an incubator at 37 °C (humidified with 5% CO_2 to confluency up to 20 days) and supplemented with DMEM consisting of 10% foetal bovine serum (Eurobio, France), 10% horse serum (Eurobio, France), 2 mM glutamine (Sigma-Aldrich, France) and 100 U/ml penicillin/streptomycin (Sigma-Aldrich, France) prior use.

Cells exposure to nanosized zeolites: Before to cells exposure the Na-X and Cu-X nanozeolites were diluted in culture medium at concentrations: 1, 10, 50 or 100 μg/ml then added directly into the wells. Cells were exposed to nanozeolites for a period of 24, 48 and 72h. The control tests were performed with distilled water under exactly the same conditions.

Cells viability: Cells were seeded in 24-wells plates to obtain 80% of confluence on the day of analysis and measured in compliance with manufacturer's manual (WST-1 assay, Roche, France).

3 Results and discussion

3.1 Properties of prepared nanozeolites

The synthesised Na-X nanosized zeolite sample is pure and highly crystalline (Figure 1 (a,b,c). After ion-exchange with copper the framework structure of the sample Cu-X is completely preserved. The X-ray diffraction patterns of Na-X and Cu-X are alike in nature and typical for FAU-type zeolite. Figure 1a illustrates the Bragg peaks widening, which indicates the small size of zeolite crystals. The morphology of prepared samples was further assessed by TEM, which confirmed the nanosized particle size with mean diameter < 40 nm (Figure 1a and b). The homogeneous nanocrystals exhibit a typical octahedral morphology with fully crystalline and well-developed faces, which remained unchanged after the incorporation of copper .

The elemental composition of the samples is presented in Table 1. The ion-exchange process does not influence the Si/Al ratio, which was around 1.6 for both samples. Consequently, 59 % of sodium was exchanged, leaving 5.11 wt % of copper present in the Cu-X sample.

The stability of colloidal zeolite suspensions is one of the prime factors considered for biomedical applications. The stability of Na-X and Cu-X samples is determined by evaluating the zeta potential values. This technique measures the surface charge of nanoparticles and it is influenced by pH/concentration of the zeolite suspension.

Generally, the zeta potential limit value of ±30 mV is employed to determine the stability of nanozeolites in suspension. The zeta potential values are -43.1 mV to -42.4 mV for Na-X and Cu-X nanozeolites, respectively, demonstrating the high colloidal stability of both zeolite suspensions (Figure 2a). In addition, DLS results show narrow, monomodal particle size distribution, which are similar for both samples (Figure 2b). This indicates that the ion-exchange does not influence the stability of zeolite nanocrystals.

Table 1. The elemental analysis of Na-X and Cu-X zeolites determined by ICP.

Sample name	Na (wt. %)	Cu (wt. %)	Al (wt. %)	Si (wt. %)	Si/Al
Na-X	9.60	-	11.84	19.29	1.63
Cu-X	5.69	5.11	11.38	17.86	1.57

3.2. In-situ FTIR measurements

In-situ IR spectroscopy was used to determine the sorption capacity of as-prepared Na-X and Cu-X samples toward NO and CO_2.

The adsorption of nitric oxide on zeolite samples after activation was performed at room temperature. The IR spectra of NO adsorbed on Na-X and Cu-X in the region of 1652-1260 cm^{-1} are presented in Figure 3. The spectra are similar with the exception of the bands at 1906 and 1883 cm^{-1} clearly observed in the Cu-X sample (Figure 3b).

According to previous studies the bands positioned in the 1652-1260 cm^{-1} region correspond to surface species, in most cases nitrates, nitrites and nitro and/or nitrito compounds (Table 2) [37–40]. The bands at 1906 and 1883 cm^{-1} are attributed to

nitrosyls, which are formed upon nitric oxide adsorption on two different Cu^{2+} sites, giving rise to formation of Cu^{2+}–NO species. No bands at 1900 cm^{-1} was observed for pure Na-X nanozeolite.

The adsorption capacity of zeolites towards NO was evaluated by measuring the intensity of the bands in the region of 1906 - 1883 cm^{-1} at 100 Torr (Figure 4). The results indicated that copper-containing nanozeolite has greater NO capacity in comparison to the Na-X. This can be explained by the stronger interactions of NO with the copper by the formation of new adsorption sites for NO.

Table 2. Assignment of the IR bands observed after NO adsorption on Na- and Cu-X.[36,37]

IR bands (cm^{-1})	**Structure**	**Notes**
1906	NO on Cu^{2+}	on Cu^{2+} carrying extra lattice oxygen
1883	NO on Cu^{2+}	on isolated Cu^{2+} moved to accessible position
1652-1649	bridging nitrates	on Al sites
1579-1554	monodentate nitrates	on Si sites
1486	monodentate nitrate	-
1442	monodentate nitrito	-
1404	nitrate species	-
1379-1353	Nitro species	-
1315	Nitro/nitrate species	-
1260	Nitro species	on Na sites

The adsorption of carbon dioxide was carried out at room temperature on the readily activated Na- and Cu-X zeolite samples. Figure 5a, b presents the evolution of FTIR spectra for Na-X and Cu-X nanozeolites. Two regions at 2400-2300 cm^{-1} and 1800-1200 cm^{-1} were evaluated. These regions are characteristic for physisorbed and chemisorbed CO_2 species, respectively. Accordingly, well-pronounced adsorption bands at 2353 cm^{-1} and 2350 cm^{-1} are present for Na-X and Cu-X, which are ascribed to the

asymmetric stretching mode of physically adsorbed carbon dioxide on the zeolite surface [41].

The band intensity increases with increasing gas pressure, therefore the amount of physisorbed CO_2 was evaluated at constant pressure for both samples. The spectra of sodium and copper nanozeolites at 180 Torr are presented in Figure 6 (left). The physisorbed CO_2 on the Na-X sample is eight times higher than on the Cu-X as shown in Figure 6 (right).

The less pronounced bands in the 1800-1200 cm^{-1} region are typical for carbonates [42]. These carbonate species include notably stable mono-, uni- and bidentate carbonates, which are formed as a result of CO_2 interaction with the oxygen bridging aluminium or silicon atoms [43]. It was previously reported that the carbonate formation can limit carbon dioxide adsorption due to decrease of accessibility to zeolite surface [44]. In the copper-containing sample the carbonate region is not very prominent, this made it difficult to distinguish between different types of carbonates present. The amount of chemisorbed CO_2 was measured at 180 Torr for Na-X and Cu-X, showing that sodium-containing nanosized zeolite has three times greater adsorption capacity in contrast to the copper one (Figure 6). This result demonstrates that by simple ion-exchange the properties of zeolite can be readily modified depending on the desired application. As mentioned before the adsorption of both gases was performed in the absence of water which simplified the measurements. However, when a very hydrophilic zeolite such as FAU is considered for a gas delivery in biological systems, the contact with water is unavoidable. Generally, the gas release in zeolites is stimulated by water diffusion, and other factors such as metal type, position and distribution in

zeolites have to be considered. Therefore, the evaluation of gas adsorption in hydrated sample is a challenge that has to be taken into consideration for future studies.

3.3. Cytotoxicity tests of nanosized Na-X and Cu-X zeolites

In order to assess the biocompatibility of nanozeolites and thus prove their applicability in biomedicine, cytotoxicity measurements were performed. Different cell lines including human glioblastoma (U87-MG), human kidney (HEK 293) and mice astrocytes were exposed to zeolite samples at increasing concentrations (1-100 μg/ml) for 24-72 hours, followed by cell viability measurements. It is important to note that in some cases the cell viability is greater than 100 % due to cell peroliferation (increase in cell number due to cell growth and division). As a result, no toxicity was observed for U87-MG cells which were subjected to both, Na-X and Cu-X nanosized zeolites (Figure 7) whatever the concentration used until 48 h of exposure. The only exception is a small decrease in cell viability after 72 hrs of exposure to high concentration of copper-containing nanozeolites.

Human kidney cells display slightly higher sensitivity towards nanozeolites (Figure 8). In general, both zeolites are harmless to the HEK 293 cells when exposed to low concentrations, however, a 40 % decrease in cell viability was observed after 72 hrs at 100 μg/ml of Cu-X. For astrocytes cell lines exposed to zeolite nanocrystals a dose dependant cell death is observed. The cell viability decreased by ~43 % after exposure to 50-100 μg/ml of zeolites as presented in Figure 9.

4. Conclusions

The sodium- and copper-containing nanosized FAU zeolite crystals (Na-X and Cu-X) were prepared in the form of stable colloidal suspensions. The gas adsorption properties of both materials towards nitric oxide and carbon dioxide were evaluated; the materials are considered to be used for potential gas delivery systems in biomedicine. The copper ion-exchanged nanozeolites (Cu-X) show increased NO adsorption capacity due to the formation of new adsorption sites of NO in comparison to the sodium form. On the other hand the Na-X shows better adsorption affinity towards CO_2. Both, Na- and Cu-X nanozeolites, show no cytotoxicity towards human glioblastoma, kidney and mice astrocytes, confirming their biocompatibility and thus ability to be further employed as gas carriers for biomedical applications.

Acknowledgements

This work was supported by the Institut National du Cancer (PLBIO17 INCA_11699) and Conseil Régional de Basse-Normandie (Projet Emergence ZEOXY) France), and the European Union-Fonds Européen de Développement Régional (FEDER)

5. References

[1] M. Iwamoto, S. Yokoo, K. Sakai, S. Kagawa, J. Chem. Soc. Faraday Trans. 1 Phys. Chem. Condens. Phases 77 (1981) 1629-1638.

[2] P. Ciambelli, P. Corbo, F. Migliardini, Catal. Today 59 (2000) 279–286.

[3] G. Delahay, S. Kieger, N. Tanchoux, P. Trens, B. Coq, Appl. Catal. B Environ. 52 (2004) 251–257.

[4] C. Boruban, E. Nalbant Esenturk, J. Mater. Res. 32 (2017) 3669–3678.

[5] M.R. Hudson, W.L. Queen, J.A. Mason, D.W. Fickel, R.F. Lobo, C.M. Brown, J. Am. Chem. Soc. 134 (2012) 1970–1973.

[6] P.A. Bachmann, P.L. Luisi, J. Lang, Nature 357 (1992) 57–59.

[7] V. Calabrese, C. Mancuso, M. Calvani, E. Rizzarelli, D.A. Butterfield, A.M. Giuffrida Stella, Nat. Rev. Neurosci. 8 (2007) 766–775.

[8] F.X. Guix, I. Uribesalgo, M. Coma, F.J. Muñoz, Prog. Neurobiol. 76 (2005) 126–152.

[9] A. Chakhoyan, A. Corroyer-Dulmont, M.M. Leblond, A. Gérault, J. Toutain, L. Chazaviel, D. Divoux, E. Petit, E.T. MacKenzie, F. Kauffmann, N. Delcroix, M. Bernaudin, O. Touzani, S. Valable, J. Cereb. Blood Flow Metab. 37 (2016) 2270–2282.

[10] J.H. Kaanders, J. Bussink, A.J. Van der Kogel, Lancet Oncol. 3 (2002) 728–737.

[11] Z. Cai, S. V. Yarovoi, Z. Zhu, L. Rauova, V. Hayes, T. Lebedeva, Q. Liu, M. Poncz, G. Arepally, D.B. Cines, M.I. Greene, Nat. Commun. 6 (2015) 1–10.

[12] R.W.M. van der Maazen, H.O.M. Thijssen, J.H.A.M. Kaanders, A. de Koster, A. Keyser, M.J.J. Prick, J.A. Grotenhuis, P. Wesseling, A.J. van der Kogel, Radiother. Oncol. 35 (1995) 118–122.

[13] R.S. Drago, B.R. Karstetter, J. Am. Chem. Soc. 83 (1961) 1819–1822.

[14] K.M. Davies, D.A. Wink, J.E. Saavedra, L.K. Keefer, J. Am. Chem. Soc. 123 (2001) 5473–5481.

[15] D.J. Smith, D. Chakravarthy, S. Pulfer, M.L. Simmons, J.A. Hrabie, M.L. Citro, J.E. Saavedra, K.M. Davies, T.C. Hutsell, D.L. Mooradian, S.R. Hanson, L.K. Keefer, J. Med. Chem. 39 (1996) 1148–1156.

[16] H. Zhang, G.M. Annich, J. Miskulin, K. Stankiewicz, K. Osterholzer, S.I. Merz, R.H. Bartlett, M.E. Meyerhoff, J. Am. Chem. Soc. 125 (2003) 5015–5024.

[17] H. Zhang, G.M. Annich, J. Miskulin, K. Osterholzer, S.I. Merz, R.H. Bartlett, M.E. Meyerhoff, Biomaterials 23 (2002) 1485–1494.

[18] R.E. Morris, P.S. Wheatley, Angew. Chemie - Int. Ed. 47 (2008) 4966–4981.

[19] A.C. McKinlay, J.F. Eubank, S. Wuttke, B. Xiao, P.S. Wheatley, P. Bazin, J.C. Lavalley, M. Daturi, A. Vimont, G. De Weireld, P. Horcajada, C. Serre, R.E. Morris, Chem. Mater. 25 (2013) 1592–1599.

[20] S. Fox, T.S. Wilkinson, P.S. Wheatley, B. Xiao, R.E. Morris, A. Sutherland, A.J. Simpson, P.G. Barlow, A.R. Butler, I.L. Megson, A.G. Rossi, Acta Biomater. 6 (2010) 1515–1521.

[21] P.S. Wheatley, A.R. Butler, M.S. Crane, A.G. Rossi, I.L. Megson, R.E. Morris, Mol. Sieves From Basic Res. to Ind. Appl. Pts a B 158 (2005) 2033–2040.

[22] V. Georgieva, C. Anfray, R. Retoux, V. Valtchev, S. Valable, S. Mintova, Microporous Mesoporous Mater. 232 (2016) 256–263.

[23] L. Ohlin, P. Bazin, F. Thibault-Starzyk, J. Hedlund, M. Grahn, J. Phys. Chem. C 117 (2013) 16972–16982.

[24] G. Maurin, R. Bell, B. Kuchta, T. Poyet, P. Llewellyn, Adsorption 11 (2005)

331–336.

[25] C. Martínez, A. Corma, Coord. Chem. Rev. 255 (2011) 1558–1580.

[26] M. Zaarour, B. Dong, I. Naydenova, R. Retoux, S. Mintova, Microporous Mesoporous Mater. 189 (2014) 11–21.

[27] V. Georgieva, C. Anfray, R. Retoux, V. Valtchev, S. Valable, S. Mintova, Microporous Mesoporous Mater. 232 (2016) 256–263.

[28] S. Komaty, C. Anfray, M. Zaarour, H. Awala, V. Ruaux, S. Valable, S. Mintova, Molecules 23 (2018) 37–48.

[29] C. Anfray, B. Dong, S. Komaty, S. Mintova, S. Valable, ACS Appl Mater Interfaces 9 (2017) 13849-13854.

[30] R. Amorim, N. Vilaça, O. Martinho, R.M. Reis, M. Sardo, J. Rocha, A.M. Fonseca, F. Baltazar, I.C. Neves, J. Phys. Chem. C 116 (2012) 25642–25650.

[31] D.G. Fatouros, D. Douroumis, V. Nikolakis, S. Ntais, A.M. Moschovi, V. Trivedi, B. Khima, M. Roldo, H. Nazar, P.A. Cox, J. Mater. Chem. 21 (2011) 7789–7794.

[32] N. Vilaça, A.F. Machado, F. Morais-Santos, R. Amorim, A. Patrícia Neto, E. Logodin, M.F.R. Pereira, M. Sardo, J. Rocha, P. Parpot, A.M. Fonseca, F. Baltazar, I.C. Neves, RSC Adv. 7 (2017) 13104–13111.

[33] S.E. Russell, J.M. González Carballo, C. Orellana-Tavra, D. Fairen-Jimenez, R.E. Morris, Dalt. Trans. 46 (2017) 3915–3920.

[34] P.S. Wheatley, A.R. Butler, M.S. Crane, S. Fox, B. Xiao, A.G. Rossi, I.L. Megson, R.E. Morris, J. Am. Chem. Soc. 128 (2006) 502–509.

[35] J. Redfern, K. Goldyn, J. Verran, R. Retoux, L. Tosheva, S. Mintova, Microporous Mesoporous Mater. 253 (2017) 233–238.

[36] H. Awala, J.P. Gilson, R. Retoux, P. Boullay, J.M. Goupil, V. Valtchev, S. Mintova, Nat. Mater. 14 (2015) 447–451.

[37] M. Iwamoto, H. Yahiro, in: Handb. Zeolite Sci. Technol., New York (2003) 951–997.

[38] M. Shelef, Chem. Rev. 95 (1995) 209–225.

[39] T. Venkov, K. Hadjiivanov, D. Klissurski, Phys. Chem. Chem. Phys. 4 (2002) 2443–2448.

[40] K. Hadjiivanov, Catal. Rev. 42 (2000) 71–144.

[41] P. Galhotra, J.G. Navea, S.C. Larsen, V.H. Grassian, Energy Environ. Sci. 2 (2009) 401–409.

[42] J.W. Ward, H.W. Habgood, J. Phys. Chem. 70 (1966) 1178–1182.

[43] D. Bonenfant, M. Kharoune, P. Niquette, M. Mimeault, R. Hausler, Sci. Technol. Adv. Mater. 9 (2008) 1–7.

[44] C.L. Angell, M. V Howell, J. Phys. Chem. 47 (1969) 3831–3836.

Figure captions:

Figure 1. (a) XRD patterns of samples Na-X and Cu-X, and TEM images of (b) Na-X and (c) Cu-X.

Figure 2. (a) Zeta potential and (b) DLS curves for Na-X and Cu-X zeolite suspensions.

Figure 3. FTIR spectra evolution of NO adsorbed on (a) Na-X and (b) Cu-X nanozeolites at gas pressure varying from 1 to 100 Torr.

Figure 4. FTIR bands after NO adsorption on Na-X (black) and Cu-X (blue) at 100 Torr in the range 2075-1225 cm^{-1}.

Figure 5. FTIR spectra evolution after carbon dioxide adsorption on (a) Na-X and (b) Cu-X nanosized zeolites at room temperature.

Figure 6. FTIR spectra after carbon dioxide adsorption at 180 Torr (left) and CO2 adsorption capacity for Na- and Cu-X zeolite samples measured at 180 Torr (right).

Figure 7. (a) Representative photographs of U87-MG cells after 24 hrs exposure to 10 µg/ml of Na-X, Cu-X zeolites and control (H_2O), scale bar = 100µm. (b) Quantification of cell viability of human glioblastoma after 24, 48 and 72 hrs exposure to Na-X and Cu-X zeolites with four different concentrations. Cell viability was assessed using the WST-1 test. Mean SD. n = 3.

Figure 8. (a) Representative photographs of HEK 293 cells after 24 hrs exposure to 10µg/ml of Na-X, Cu-X zeolites and control (H_2O), scale bar = 100µm. (b) Quantification of cell viability of human glioblastoma after 24, 48 and 72 hrs exposure to Na-X and Cu-X zeolites with four different concentrations. Cell viability was assessed using the WST-1 test. Mean SD. n = 3.

Figure 9. (a) Representative photographs of astrocytes after 24 hrs exposure to 10μg/ml of Na-X, Cu-X zeolites and control (H_2O), scale bar = 100μm. (b) Quantification of cell viability of mice astrocytes after 24, 48 and 72 hrs exposure to Na-X and Cu-X zeolites with four different concentrations. Cell viability was assessed using the WST-1 test. Mean SD. n = 3.

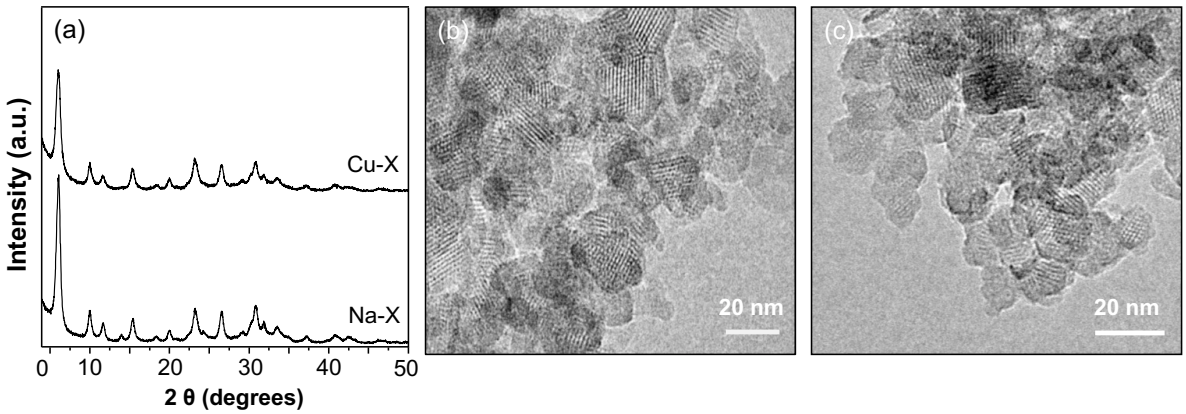

Figure 1

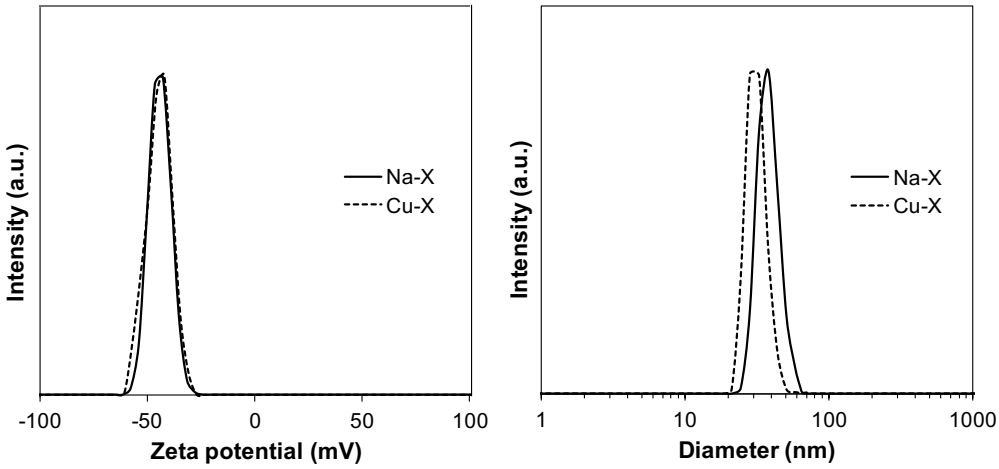
Intensity (a.u.)
Na-X
Cu-X
-100
-50
0
50
100
Zeta potential (mV)
Intensity (a.u.)
Na-X
Cu-X
1
10
100
1000
Diameter (nm)

Figure 2

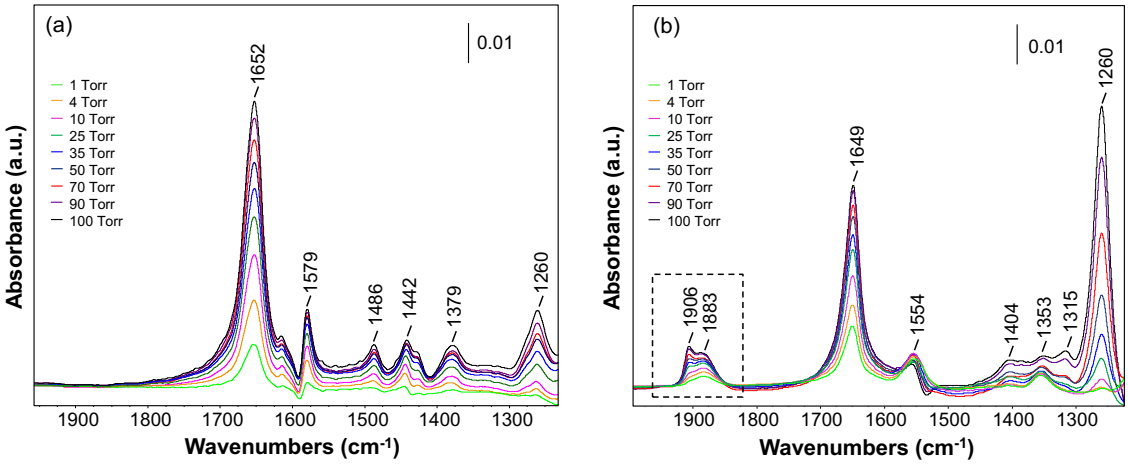
(a)
0.01
1 Torr
4 Torr
10 Torr
25 Torr
35 Torr
50 Torr
70 Torr
90 Torr
100 Torr
1652
1579
1486
1442
1379
1260
Absorbance (a.u.)
1900
1800
1700
1600
1500
1400
1300
Wavenumbers (cm-1)
(b)
0.01
1 Torr
4 Torr
10 Torr
25 Torr
35 Torr
50 Torr
70 Torr
90 Torr
100 Torr
1649
1906
1883
1554
1404
1353
1315
1260
Absorbance (a.u.)
1900
1800
1700
1600
1500
1400
1300
Wavenumbers (cm-1)

Figure 3

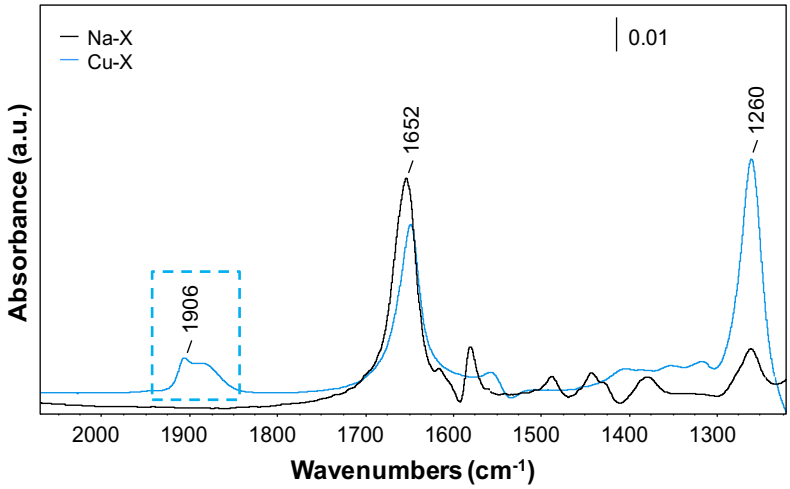
Na-X
Cu-X
0.01
1652
1260
1906
Absorbance (a.u.)
2000
1900
1800
1700
1600
1500
1400
1300
Wavenumbers (cm-1)

Figure 4

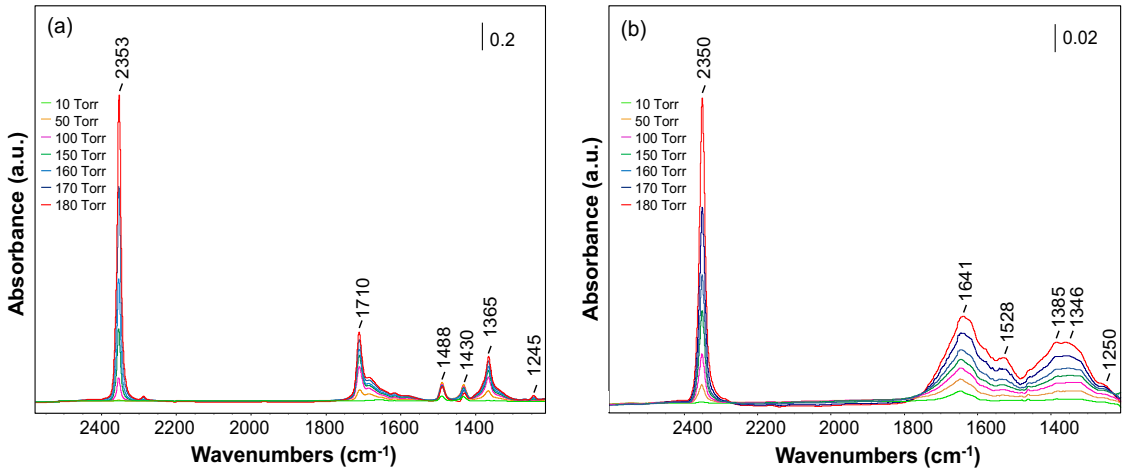
(a)
0.2
2353
1710
1488
1430
1365
1245
10 Torr
50 Torr
100 Torr
150 Torr
160 Torr
170 Torr
180 Torr
Absorbance (a.u.)
2400
2200
2000
1800
1600
1400
Wavenumbers (cm-1)
(b)
0.02
2350
1641
1528
1385
1346
1250
10 Torr
50 Torr
100 Torr
150 Torr
160 Torr
170 Torr
180 Torr
Absorbance (a.u.)
2400
2200
2000
1800
1600
1400
Wavenumbers (cm-1)

Figure 5

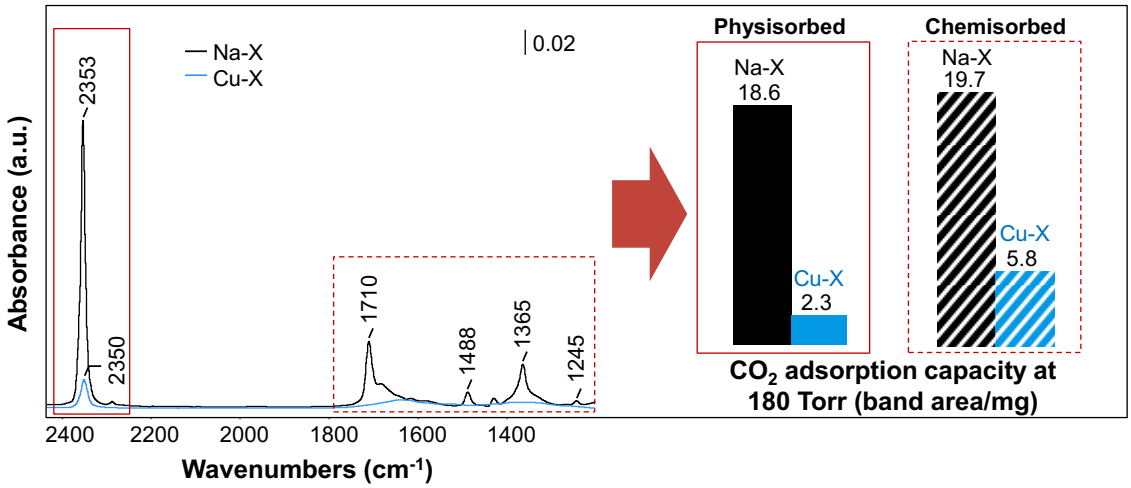
Absorbance (a.u.)
Na-X
Cu-X
0.02
2353
2350
1710
1488
1365
1245
2400
2200
2000
1800
1600
1400
Wavenumbers (cm-1)
Physisorbed
Chemisorbed
Na-X
18.6
Cu-X
2.3
Na-X
19.7
Cu-X
5.8
CO2 adsorption capacity at
180 Torr (band area/mg)

Figure 6

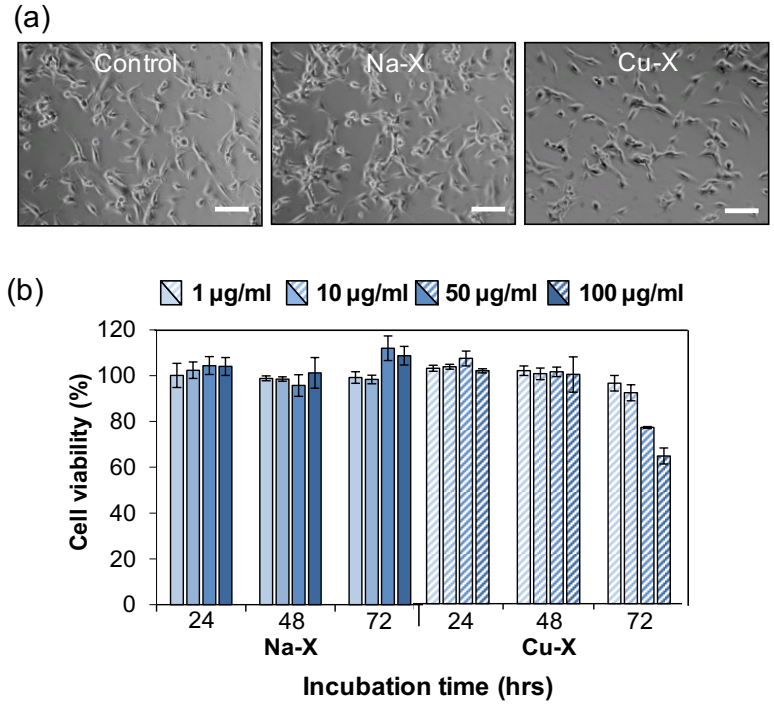
(a)
Control
Na-X
Cu-X
(b)
1 µg/ml
10 µg/ml
50 µg/ml
100 µg/ml
Cell viability (%)
120
100
80
60
40
20
0
24
48
72
24
48
72
Na-X
Cu-X
Incubation time (hrs)

Figure 7

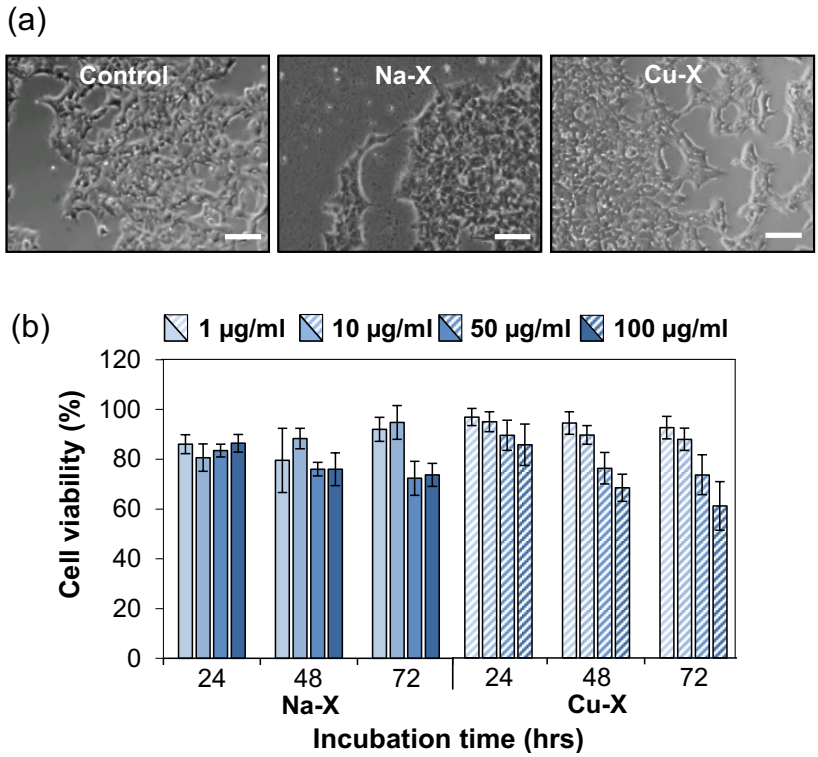
(a)
Control
Na-X
Cu-X
(b)
1 µg/ml
10 µg/ml
50 µg/ml
100 µg/ml
Cell viability (%)
120
100
80
60
40
20
0
24
48
72
24
48
72
Na-X
Cu-X
Incubation time (hrs)

Figure 8

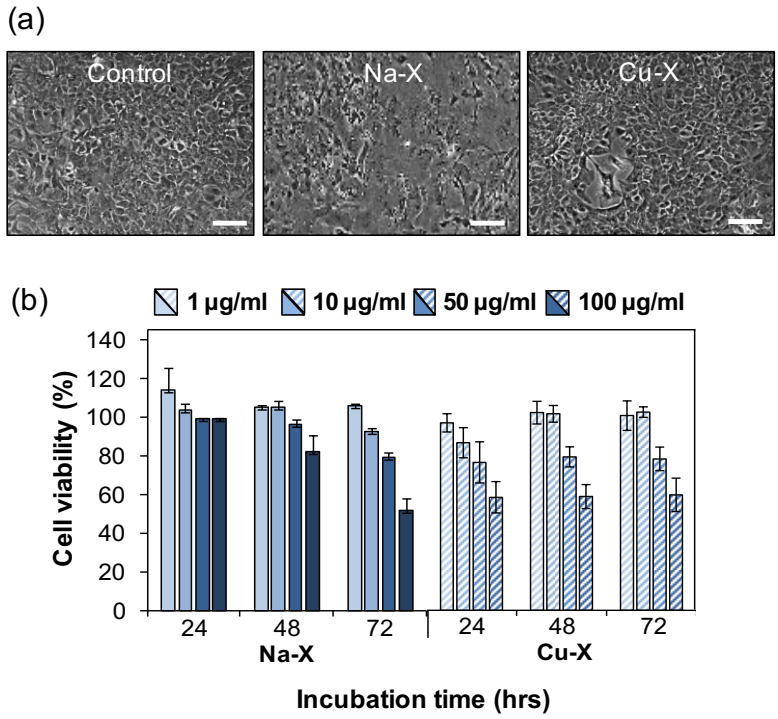
(a)
Control
Na-X
Cu-X
(b)
1 µg/ml
10 µg/ml
50 µg/ml
100 µg/ml
Cell viability (%)
140
120
100
80
60
40
20
0
24
48
72
24
48
72
Na-X
Cu-X
Incubation time (hrs)

Figure 9